J Nanostruct 15(3): 951-961, Summer 2025

RESEARCH PAPER

Synthesis, Characterization, and Biological Evaluation of Nano Schiff Base Derivatives and Their Conversion into Oxazepine and Imidazoline Derivatives: A Comprehensive Study

Manahil Saleh Abdel Amir *, May Jaleel Abed

Department of Chemistry, College of Education, University of Al-Qadisiyah, Diwaniyah, Iraq

ARTICLE INFO

Article History:
Received 10 April 2025
Accepted 14 June 2025
Published 01 July 2025

Keywords:
Anticancer activity
Imidazoline
MCF-7 cell line
Oxazepine
Schiff-base derivatives

ABSTRACT

This work synthesizes, characterizes, and biologically evaluates nano Schiff-base compounds and their transition into oxazepine and imidazoline derivatives. Under reflux conditions, aldehyde and ketone derivatives reacted with amine derivatives in absolute ethanol and glacial acetic acid. The reactions were monitored using thin-layer chromatography (TLC), and the products were recrystallized from 100% ethanol. The structural integrity of resulting compounds was confirmed using FT-IR, ^{1}H-NMR and ^{13}C-NMR spectroscopy. FT-IR analysis showed functional group modifications such NH_2 and C=N stretch band disappearance and C=O stretch band emergence. ^{1}H-NMR and ^{13}C-NMR studies gave in-depth insights into proton and carbon environments, enabling successful synthesis of target molecules. Synthesized derivatives were tested for anticancer activity using the MTT assay against MCF-7 breast cancer cells and WRL-68 normal liver cells. The results showed a dose-dependent suppression of cell proliferation, with greater derivative concentrations harmful to MCF-7 cells but less hazardous to WRL-68 cells. These half-maximal inhibitory concentration (IC50) values for compounds showed their potential as anticancer agents. XRD and FESEM analyses revealed the derivatives' crystalline structure and surface morphology. FESEM images showed particle size and surface shape, reflecting the compounds' production circumstances and probable uses. XRD patterns showed variable crystallinity.

How to cite this article
Amir M., Abed M. Synthesis, Characterization, and Biological Evaluation of Nano Schiff Base Derivatives and Their Conversion into Oxazepine and Imidazoline Derivatives: A Comprehensive Study. J Nanostruct, 2025; 15(3):951-961. DOI: 10.22052/JNS.2025.03.013

INTRODUCTION

High electron-donating and strong coordination characteristics have made heterocyclic compounds popular, and their numerous uses continue to draw attention [1]. Many methods have been found to prepare nano Schiff-bases. Schiff-bases have many biological properties and are employed in industry [2]. They are widely used as organic synthesis intermediates, catalysts, dyes, and polymer stabilizers [3]. Green chemistry's clean energy cycloaddition operations produce oxazepines with less byproducts and shorter reaction times [4]. Oxazepine derivatives are stable and biologically active due to the seven-membered ring's double bond alternation [5]. This has inspired researchers to develop novel synthesis methods for seven-membered ring compounds. Oxazepine compounds are

* *Corresponding Author Email: chem.edu.post15@qu.edu.iq*

synthesized by condensing nano Schiff-bases with phthalic anhydride. In recent years, interest in tetrazole chemistry has rapidly increased due to its applications. The first discovery of tetrazole was made by the Swedish chemist Bladin A.J. in 1896, and then, research interest in this heterocyclic system has grown, leading to its chemical and biological development [6]. Tetrazole ring systems have been extensively studied for a variety of applications in organic chemistry, coordination chemistry, photography, agriculture, explosives, and particularly in medicine, for designing numerous bioequivalents of carboxylic acids, such as 5-substituted tetrazoles and 2,5-disubstituted tetrazoles, which serve as bioequivalents of the cis-amide bond in peptides [7]. These bioequivalents play a similar role in various biological activities by enhancing wide metabolic stability, especially for their role in medicine [8]. Beta-lactams have garnered significant attention due to their antibacterial properties, in which those found in penicillin and cephalosporin, making them important classes of antibiotics in both human and veterinary medicine [9]. They represent over 85% of the global antibiotic market [10]. Additionally, they are used in other clinical applications, such as clavulanic acid as beta-lactamase inhibitors and ezetimibe as cholesterol absorption inhibitors. Beta-lactams also demonstrate other biological activities, including anti-cancer, anti-diabetic, anti-tuberculosis, and anti-inflammatory effects [11].

MATERIALS AND METHODS

Reagents and instruments

The preparation of various derivatives involved the use of the following reagents and instruments. Aldehyde and ketone derivatives, amine derivatives, absolute ethanol, glacial acetic acid, dry benzene, succinic anhydride, maleic anhydride, phthalic anhydride, tetrahydrofuran (THF), amino acids (alanine, glycine), 1,4-dioxane, thioglycolic acid, anhydrous zinc chloride, sodium azide, triethylamine, chloroacetyl chloride, and anthracitic acid were used as chemical reagents. The instruments and equipment included round-bottom flasks equipped with magnetic stirrers, conical flasks, reflux setups, thin-layer chromatography (TLC) plates, and appropriate mobile phases (such as benzene in a 4:1 ratio). The reaction mixtures were typically heated, refluxed, and monitored for progress using TLC. The resulting precipitates were filtered, dried, recrystallized from absolute ethanol, and their physical properties were determined.

Synthesis procedure

General method for preparing derivative (1)

Equimolar amounts (0.005 mol) of aldehyde and ketone derivatives were mixed with 0.005 mol of amine derivatives in a round-bottom flask equipped with a magnetic stirrer containing 30 mL of absolute ethanol. Three drops of glacial acetic acid were added to the mixture, which was then refluxed for 6 h. The reaction mixture was cooled and left to stand for 24 h. The precipitate was filtered, washed, dried, and recrystallized from absolute ethanol. The progress of the reaction was monitored using TLC with an appropriate mobile phase [1].

General method for preparing derivatives (2, 3, 4)

Nano Schiff-base derivative (1) (0.00167 mol) was dissolved in 30 mL of dry benzene. Then, 0.00167 mol of succinic anhydride, maleic anhydride, or phthalic anhydride was added. The mixture was heated at 60°C for 39 h. The reaction progress was monitored using TLC with a mobile phase of benzene (4:1). The precipitate was filtered, dried, recrystallized from absolute ethanol, weighed, and its physical properties were determined [12].

Preparation of oxazepine derivative (2)

This derivative was prepared using the general method with 0.179 g of derivative (1) and 0.24 g of phthalic anhydride under reaction time of 39 h. A yellow precipitate was obtained [13].

Preparation of oxazepine derivative (3)

This derivative was prepared using the general method with 0.5 g of derivative (1) and 0.163 g of maleic anhydride under reaction time of 39 h. An orange precipitate was obtained.

Preparation of oxazepine derivative (4)

This derivative was prepared using the general method with 0.5 g of derivative (1) and 0.190 g of succinic anhydride under reaction time of 39 h. A yellow precipitate was obtained.

Preparation of imidazoline derivatives (5)

Derivative (1) (0.926 g, 0.0031 mol) was dissolved in 30 mL of THF, along with amino acids (alanine, glycine) in a conical flask equipped with

a magnetic stirrer. The mixture was refluxed for 42-48 h, and the reaction progress was monitored using TLC with a mobile phase of benzene (4:1). The precipitate was allowed to stand for a day,

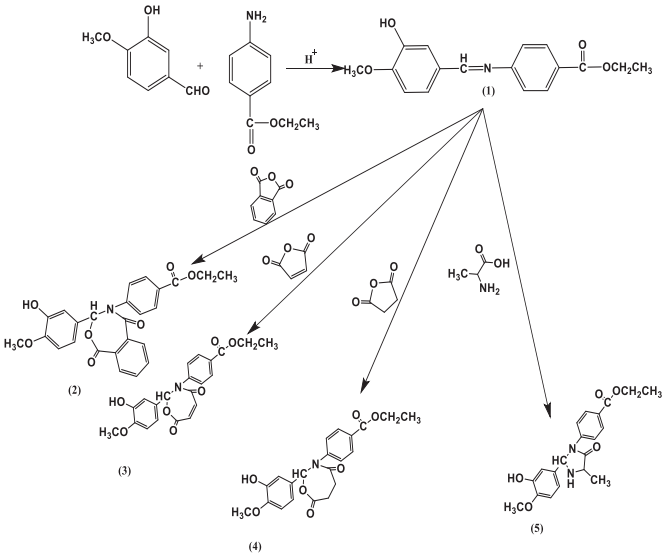

Fig. 1. Synthesis method of different derivatives (1-5).

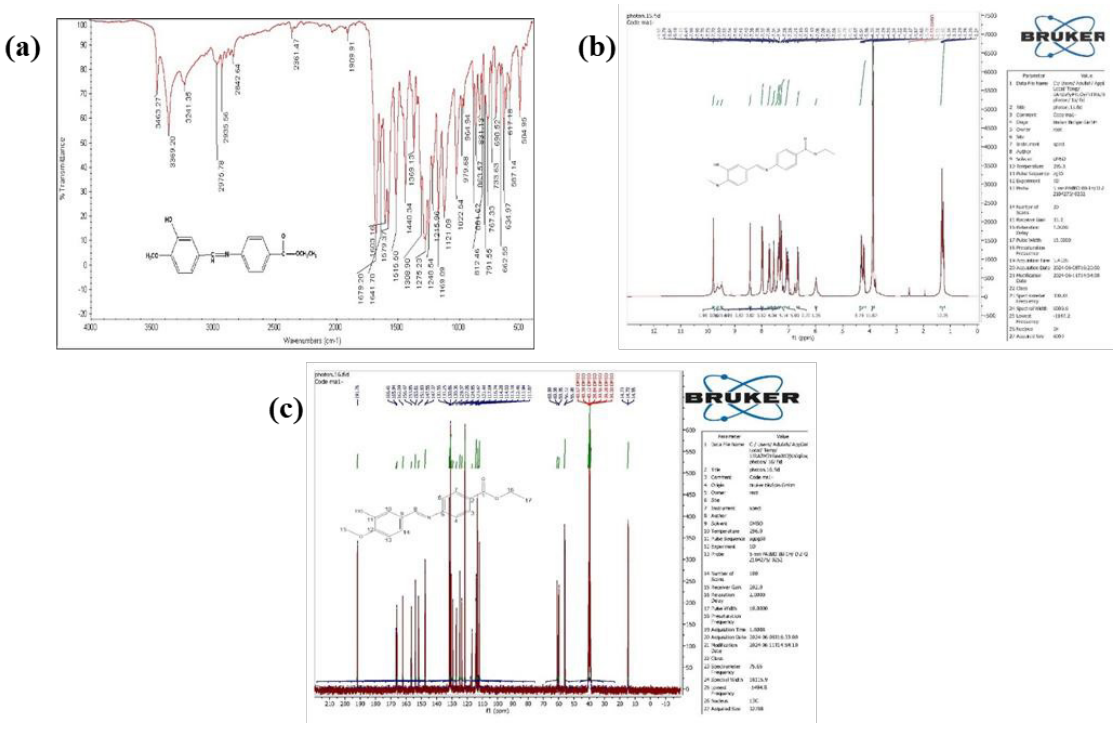

Fig. 2. (a) FT-IR, (b) ^{1}H-NMR and (c) ^{13}C-NMR spectra of derivative (1).

recrystallized from absolute ethanol, dried, and weighed (Fig. 1) [13].

RESULTS AND DISCUSSION

FT-IR, ^{1}H-NMR, and ^{13}C-NMR results

The nano Schiff-base derivative (1) was characterized by FT-IR spectroscopy, as illustrated in Fig. 2a. The NH_2 stretching band disappeared, and a new band at 1641 cm^{-1}, corresponding to the azomethine group (C=N) stretching vibration, was observed. Additionally, a signal at 3369 cm^{-1} attributed to the phenolic (O-H) stretch and a signal at 1679 cm^{-1} corresponding to the C=O stretch were detected. The characterization of compound (1) was further confirmed using ^{1}H-NMR spectroscopy with (DMSO-d_6) as the solvent. The spectrum, depicted in Fig. 2b, showed a singlet at 9.8 ppm corresponding to the hydroxyl group proton, a triplet at 1.9 ppm for the six protons of the CH_3 group, a singlet at 3.8 ppm for the three protons of the OCH_3 group, and multiple signals in the range of 6.6-7.2 ppm corresponding to the aromatic ring protons. A signal at 2.5 ppm was attributed to the solvent, (DMSO-d_6). Additionally, compound (1) was characterized using ^{13}C-NMR spectroscopy, as illustrated in Fig. 2c, which revealed a distinct signal. A signal at 180 ppm was assigned to C1, while a signal at 164 ppm corresponded to C11. The signal at 55.98 ppm was attributed to C15, and the signal at 14.70 ppm was assigned to C17. Additionally, a signal at 56.12 ppm was attributed to C8. Signals in the range of 111-166 ppm were observed for the aromatic rings [14, 15].

FT-IR spectrum of derivative (2) is depicted in Fig. 3a. The spectrum revealed a band at 3369 cm^{-1} corresponding to the phenolic O-H stretch. The disappearance of the C=N stretch band for the azomethine group and the appearance of a band at 1679 cm^{-1} for the C=O stretch of the oxazepine ring were observed. Additionally, a band at 1642 cm^{-1} was assigned to the C=O stretch. Compound (2) was further characterized by ^{1}H-NMR spectroscopy using DMSO-d_6 as the solvent. The spectrum in Fig. 3b displayed a singlet at 9.7 ppm attributed to the hydroxyl group proton, a triplet at 1.3 ppm corresponding to the six protons of the CH_3 group, and a singlet at 3.87 ppm for the three protons of the OCH_3 group. Multiplets in the range

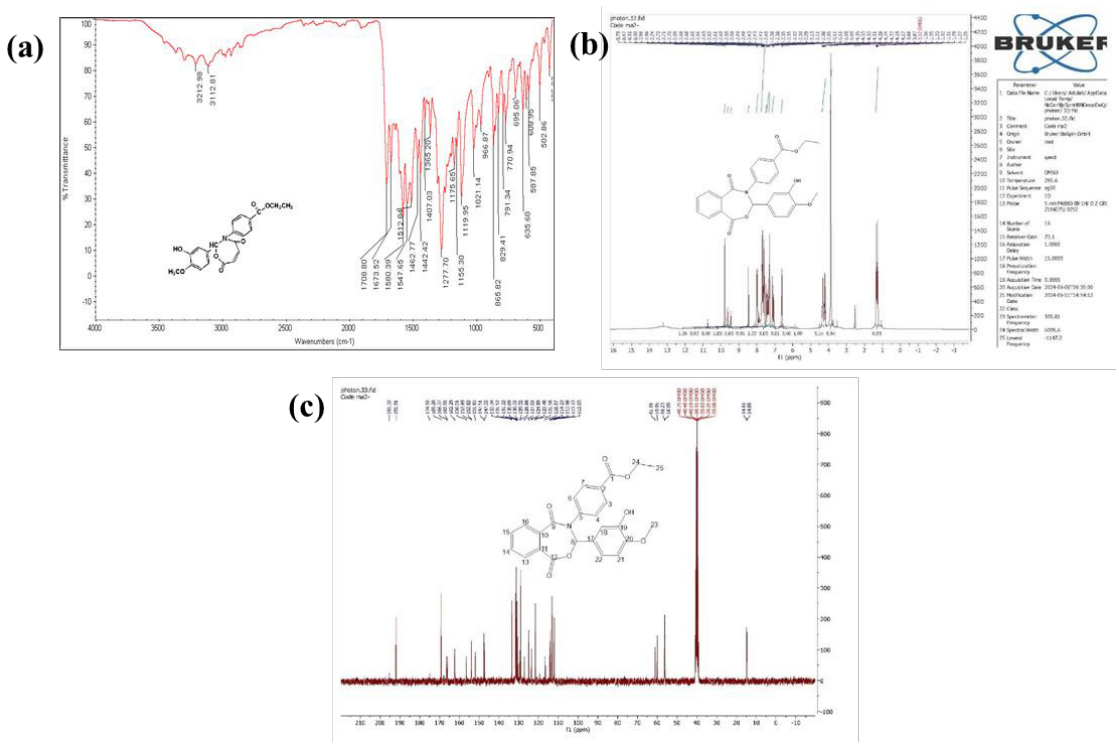

Fig. 3. (a) FT-IR, (b) ^{1}H-NMR and (c) ^{13}C-NMR spectra of derivative (2).

of 7.3-6.5 ppm were assigned to the aromatic ring protons. An additional signal at 2.5 ppm was due to the solvent (DMSO-d_6). 13C-NMR spectroscopy was also employed to characterize compound (2). The spectrum in Fig. 3c exhibited a signal at 195 ppm corresponding to C1, signals in the range of 174-191 ppm for C9 and C12, and a signal at 166 ppm for C19. Signals at 14.56 and 14.28 ppm were assigned to C23 and C25, respectively. A signal at 55 ppm corresponded to C24, while signals in the range of 112-165 ppm were attributed to the aromatic rings [16].

The characterization of derivative (3) was carried out using FT-IR spectroscopy, as illustrated in Fig. 4a. The spectrum indicated the disappearance of the C=N stretch band of the azomethine group and the appearance of a band at 3307 cm^{-1} corresponding to the phenolic O-H stretch. A band at 1708.8 cm^{-1} was assigned to the C=O stretch, and another band at 1673 cm^{-1} was attributed to the C=O stretch vibration. Further analysis was conducted using ^{1}H-NMR spectroscopy with DMSO-d_6 as the solvent. The ^{1}H-NMR spectrum in Fig. 4b exhibited a singlet at 10 ppm attributed to the hydroxyl group proton, a triplet at 1.3 ppm corresponding to the six protons of the CH_3 group, and a singlet at 3.87 ppm for the three protons of the OCH_3 group. Multiplets in the range of 6.2-7.08 ppm were assigned to the aromatic ring protons. An additional signal at 2.5 ppm was due to the solvent (DMSO-d_6). ^{13}C-NMR spectroscopy was also utilized to characterize compound (3). The ^{13}C-NMR spectrum in Fig. 4c showed a signal at 191.9 ppm corresponding to C1, signals at 188 ppm and 182 ppm for C9 and C12, respectively, and a signal at 170 ppm for C14. A signal at 14.82 ppm was assigned to C23, while another at 14.66 ppm was attributed to C21. A signal at 56 ppm corresponded to C20, with additional signals in the range of 112-165 ppm are attributed to the aromatic rings [17, 18].

FT-IR spectrum of derivative (4) is depicted in

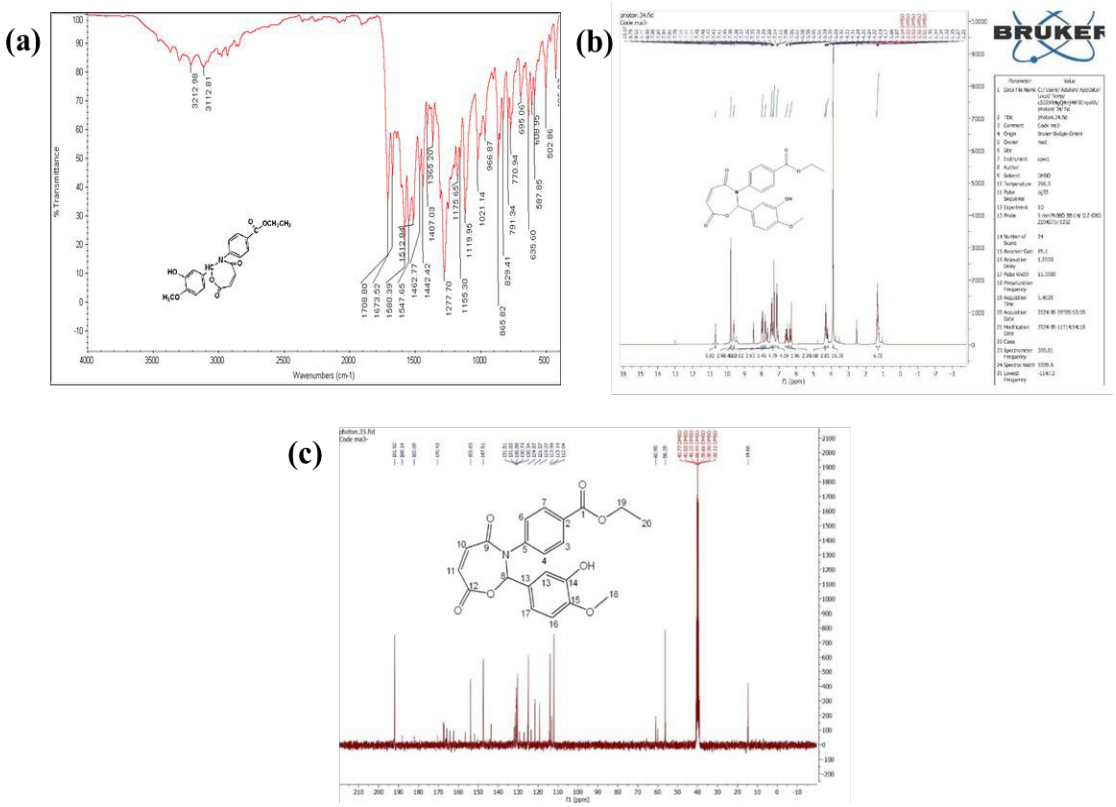

Fig. 4. (a) FT-IR, (b) ^{1}H-NMR and (c) ^{13}C-NMR spectra of derivative (3).

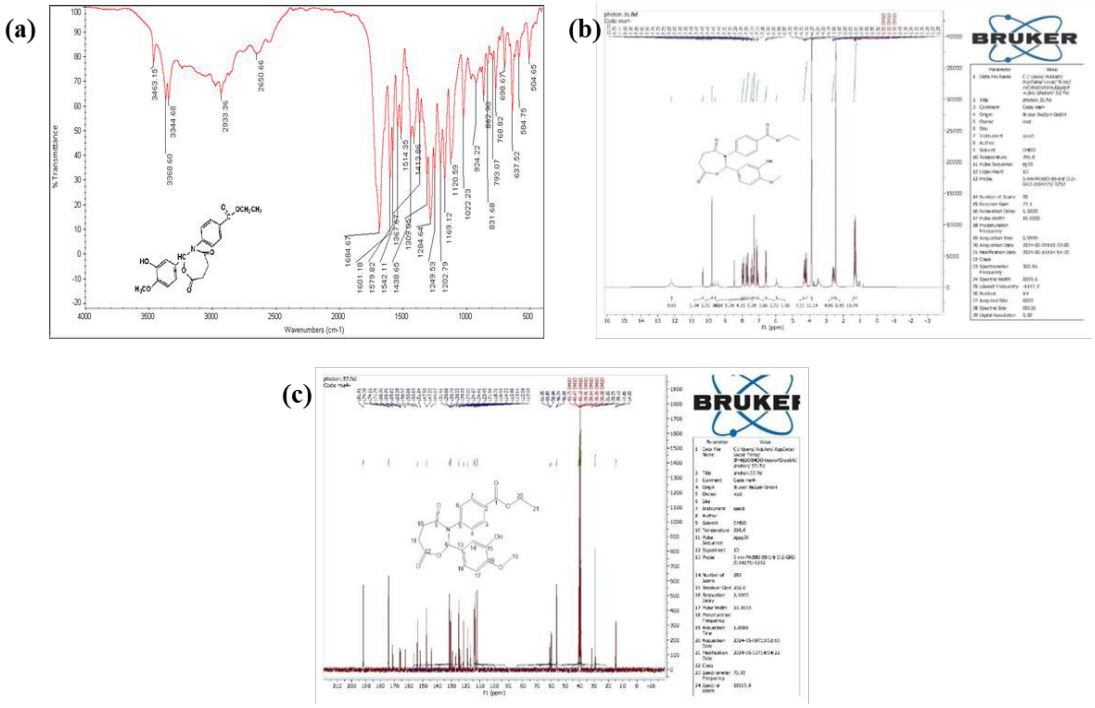

Fig. 5. (a) FT-IR, (b) ^{1}H-NMR and (c) ^{13}C-NMR spectra of derivative (4).

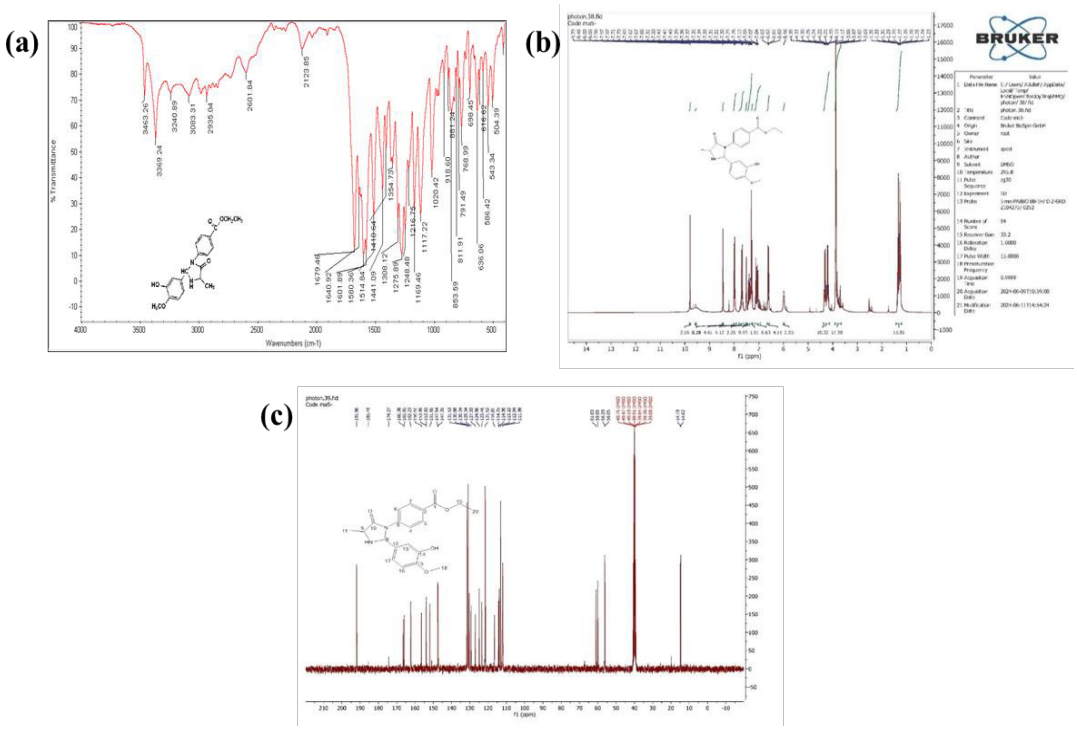

Fig. 6. (a) FT-IR, (b) ^{1}H-NMR and (c) ^{13}C-NMR spectra of derivative (5)

Fig. 5a. The spectrum indicated the disappearance of the C=N stretch band of the azomethine group and the appearance of a band at 3368 cm^{-1} corresponding to the phenolic O-H stretch. A band at 1684 cm^{-1} is attributed to the C=O stretch. Compound (4) was further characterized by ^{1}H-NMR spectroscopy using DMSO-d_6 as solvent. The spectrum in Fig. 5b exhibited a singlet at 10.33 ppm attributed to the hydroxyl group proton, a triplet at 2.6 ppm corresponding to the protons of the CH_3 group, and a singlet at 3.87 ppm for the three protons of the OCH_3 group. Multiplets in the range of 6.5-7.28 ppm were assigned to the aromatic ring protons. An additional signal at 2.5 ppm was due to the solvent (DMSO-d_6). ^{13}C-NMR spectroscopy was also utilized to characterize compound 4. The spectrum in Fig. 5c showed a signal at 191.9 ppm corresponding to C1, signals at 174.1 ppm and 174.2 ppm for C9 and C12, respectively, and a signal at 165 ppm for C8. A signal at 14.82 ppm was assigned to C21, while another at 14.66 ppm was also attributed to C21. A signal at 56 ppm corresponded to C20, with additional signals in the range of 112-171 ppm attributed to the aromatic rings [19].

FT-IR spectrum of derivative (5) is depicted in Fig. 6a. The spectrum indicated the disappearance of the C=N stretch band of the azomethine group and the appearance of a band at 3369 cm^{-1} corresponding to the phenolic O-H stretch [20-22]. Additionally, a band at 3083 cm^{-1} was observed for the aromatic C-H stretch, a band at 2935 cm^{-1} for the aliphatic C-H stretch, and a band at 1679 cm^{-1} for the C=O stretch. Compound (5) was further characterized by ^{1}H-NMR spectroscopy using DMSO-d_6 as the solvent. The spectrum in Fig. 6b exhibited a singlet at 9.79 ppm attributed to the hydroxyl group proton, a triplet at 1.26 ppm corresponding to the six protons of the CH_3 group, and a singlet at 3.87 ppm for the three protons of the OCH_3 group. Multiples in the range of 6.6-7.37 ppm were assigned to the aromatic ring protons. An additional signal at 2.5 ppm was due to the solvent (DMSO-d_6). ^{13}C-NMR spectroscopy was also utilized to characterize compound (5). The spectrum in Fig. 6c showed a signal at 191 ppm

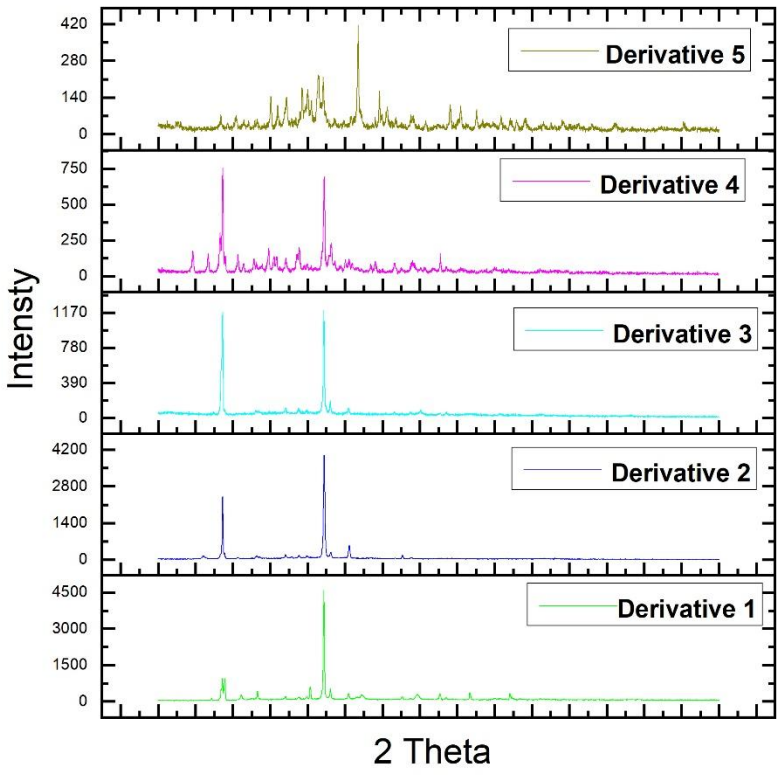

Fig. 7. XRD patterns of different derivatives (1-5).

for C1, a signal at 185 ppm for C10, and a signal at 174 ppm for C14. Additional signals in the range of 111-166 ppm were attributed to the aromatic rings [23].

XRD study

The XRD patterns provided the structural analysis of five synthesized organic compounds, labeled as derivatives 1-5 (Fig. 7). These patterns displayed the intensity of diffracted X-rays as a function of the diffraction angle (2 Theta), revealing crucial information about the crystalline structure and phase purity of the compounds [24-28]. Derivatives (1) and (2) exhibit sharp and intense peaks, indicating high crystallinity and phase purity. Derivative (3) shows sharp peaks with slightly lower intensity, suggesting minor differences in crystal quality. Derivative (4) has

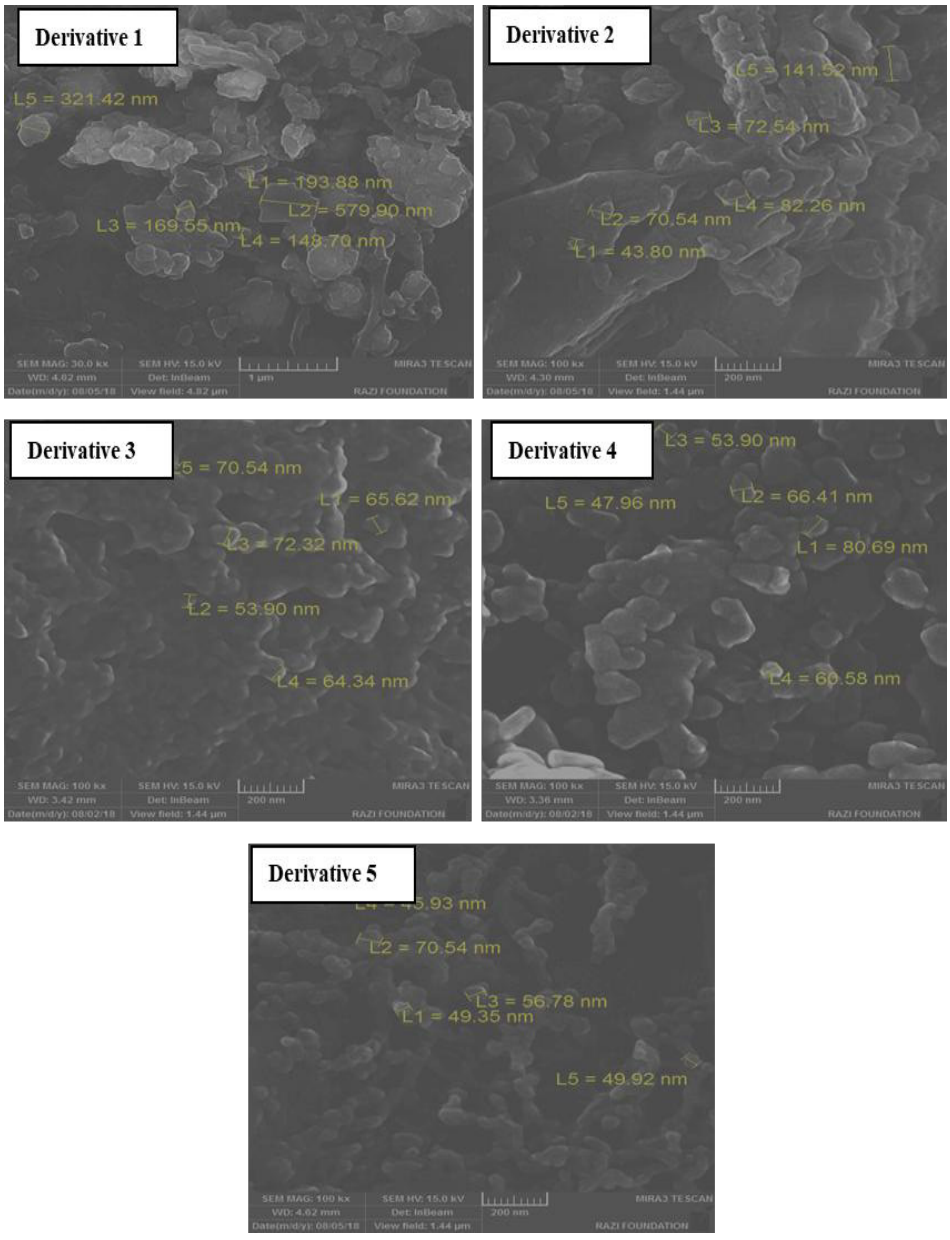

Fig. 8. FESEM images of derivatives (1-5).

multiple peaks with reduced intensity, indicating a semi-crystalline structure. Derivative (5) features numerous low-intensity peaks, signifying reduced crystallinity and increased amorphous content. Recent research extensively uses XRD analysis to characterize synthesized organic compounds, confirming successful synthesis and purity by comparing experimental patterns with standard references. Sharp peaks correlate with high crystallinity, associated with better stability and performance. Each derivative is uniquely identified by its structural formula. This synthesis and structural characterization align with global research practices, where XRD is fundamental in elucidating the structural properties of newly synthesized compounds [29-31].

FESEM analysis

The FESEM images in Fig. 8 provide detailed insights into the surface morphology and particle size distribution of the five synthesized nano organic compounds. Derivative (1) shows a relatively uniform surface with well-defined particles ranging from approximately 50 to 321 nm, suggesting a controlled synthesis process with some variation in particle size. Derivative (2) has a slightly rougher surface with irregularly shaped particles ranging from about 44 nm to 173 nm, indicating slight variations in synthesis parameters or chemical composition. Derivative (3) displays

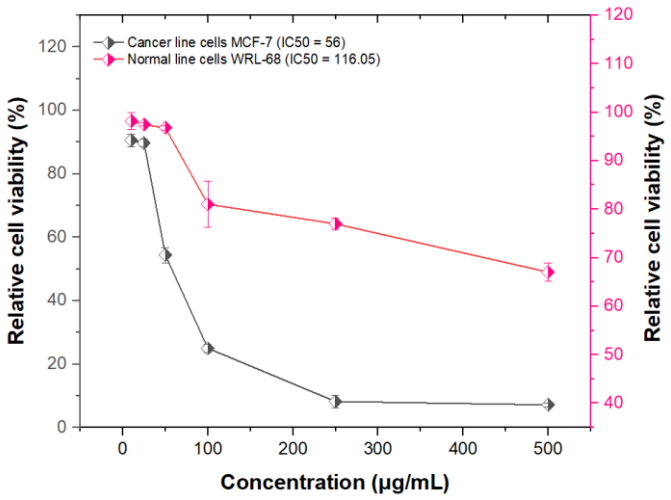

Fig. 9. The relationship between the biological activity of MCF-7 breast cancer cell line and WRL-68 normal cell line against the concentration of derivative (5)

Table 1. Evaluation of the cytotoxicity of derivative (5) against the MCF-7 cancer cell line and WRL-68 cell line after incubation for 24 h at a temperature of 37 °C.

Concentration (µg/mL)	Derivative (5)					
	Cancer line cells MCF-7			Normal line cells WRL-68		
	Cell Viability		%Cell inhibition	Cell Viability		%Cell inhibition
	Mean	SD		Mean	SD	
10	90.53287	1.950846	9.46712	98.20537	1.772750	1.79462
25	89.71088	1.20556	10.28911	97.43996	0.304971	2.56003
50	54.36281	2.37842	17.97052	96.77515	0.448983	3.22484
100	24.97959	1.26982	34.3537	81.03847	4.76494	18.96152
250	8.19387	2.03193	61.13945	76.98748	1.184553	23.01251
500	7.14285	0.64199	92.85714	67.02271	1.911425	32.97728
IC50		56			116.05	

a broad size distribution of particles from 54 nm to 170 nm, suggesting a less controlled synthesis environment and different crystalline phases. Derivative (4) exhibits a more aggregated structure with interconnected particles forming a porous network, with sizes ranging from approximately 53 nm to 70 nm, indicating a rough and textured surface potentially beneficial for catalysis or adsorption. Derivative (5) has a highly irregular and rough surface morphology with particle sizes ranging from 49 nm to 97 nm, indicating the least uniformity among the samples and potential challenges in the synthesis process. Overall, the FESEM analysis provides critical information about the surface characteristics and particle size of the synthesized compounds, essential for understanding their potential applications and performance in various fields. The observed variations in particle size and morphology reflect the different synthesis conditions and potential applications of each derivative [32-36].

Anticancer activity

The effects of derivative (5) on the growth of the MCF-7 cell line and the WRL-68 cells were studied, showing a similar trend with the lowest growth inhibition at 10 µg/mL and the highest at 500 µg/mL for both cell lines [37, 38]. The WRL-68 cells were used for comparison and potential medical application. The percentage of live cells remaining after treatment with derivative (5) ranged from 7.14285% to 90.53287% for the MCF-7 cell line, and from 67.02271% to 98.20537% for the WRL-68 cell line. The highest inhibition rate for the MCF-7 cell line was 92.85714% at 500 µg/mL, while for the WRL-68 cell line, it was 32.97728% at the same concentration. The IC50 for derivative (5) with the MCF-7 cell line was 56 µg/mL, and for the WRL-68 cells, it was 116.5 µg/mL, as summarized in Table 1 and Fig. 9 [39-41].

CONCLUSION

This study used FT-IR, ^{1}H-NMR, and ^{13}C-NMR to characterize chemical derivatives. These compounds have unique chemical and physical properties, making them promising for industrial and medical uses. These derivatives' surface morphology and particle size distribution were examined using FESEM. Shapes and sizes varied due to synthesis circumstances. This information is essential for understanding these compounds' catalytic and adsorption applications. Compound (5) was tested for anticancer activities in MCF-7 breast cancer and WRL-68 normal liver cells. Results demonstrated substantial anticancer action with reduced influence on normal cells, suggesting therapeutic potential. The purity and crystallinity of these derivatives were examined using XRD patterns. This clarifies the link between crystalline structure and compound physical and chemical properties. This study shows that these compounds have great industrial and medical potential. It emphasizes the need for ongoing R&D to improve characteristics and find new uses.

CONFLICT OF INTEREST

The authors declare that there is no conflict of interests regarding the publication of this manuscript.

REFERENCES

1. Joule JA, Mills K. Heterocyclic Chemistry at a Glance: Wiley; 2012 2012/08/06.
2. Badwaik VB, Aswar AS. Synthesis, characterization, and biological studies of some Schiff base complexes. Russian Journal of Coordination Chemistry. 2007;33(10):755-760.
3. Hadjoudis E, Mavridis IM. Photochromism and thermochromism of Schiff bases in the solid state: structural aspects. Chem Soc Rev. 2004.
4. Heravi MM, Ahmadi T, Ghavidel M, Heidari B, Hamidi H. Recent applications of the hetero Diels–Alder reaction in the total synthesis of natural products. RSC Advances. 2015;5(123):101999-102075.
5. Singh SK, Mishra N, Nayak G, Mehta P. Synthesis of Schiff bases Derivatives of 1,3-oxazepine and Evaluation of Antioxidant Action In vitro. Oriental Journal Of Chemistry. 2023;39(5):1367-1372.
6. Benson FR. The Chemistry of the Tetrazoles. Chem Rev. 1947;41(1):1-61.
7. Ma J-A, Cahard D. Asymmetric Fluorination, Trifluoromethylation, and Perfluoroalkylation Reactions. Chem Rev. 2004;104(12):6119-6146.
8. Yuan Y, Li M, Apostolopoulos V, Matsoukas J, Wolf WM, Blaskovich MAT, et al. Tetrazoles: A multi-potent motif in drug design. Eur J Med Chem. 2024;279:116870.
9. Livermore DM. beta-Lactamases in laboratory and clinical resistance. Clin Microbiol Rev. 1995;8(4):557-584.
10. Kohanski MA, Dwyer DJ, Collins JJ. How antibiotics kill bacteria: from targets to networks. Nature Reviews Microbiology. 2010;8(6):423-435.
11. Elahpour N, Niesner I, Abdellaoui N, Holzapfel BM, Gritsch L, Jallot E, et al. Antibacterial Therapeutic Ions Incorporation into Bioactive Glasses as a Winning Strategy against Antibiotic Resistance. Advanced Materials Interfaces. 2024;11(32).
12. Synthesis and Estimation of Biological Activity of New Oxazepine Derivatives. International Journal of Pharmaceutical Research. 2020;12(sp2).
13. Synthesis and Characterization of Schiff Bases Derived from 1-Naphthylamine Hydrochloride, Syria: Homs. Chemistry and Materials Research. 2021.
14. Kaya İ, Kolcu F, Süel S. Synthesis and Characterization of

Schiff Base Compounds Containing Mono and Disulfonic Groups. Celal Bayar Üniversitesi Fen Bilimleri Dergisi. 2024;20(4):101-106.
15. Çelik F. New 1H-1,2,3-triazole derivatives: Synthesis, Characterization and Antioxidant Activity. Turkish Journal of Analytical Chemistry. 2025;7(2):191-194.
16. Sarı A, Çukurovalı A. The Effects of Thiosemicarbazone Derivative Schiff Base 1-(1-Phenil-1-Methylcyclobutane-3-Yl)-2-Suksinimido Etanon Thiosemicarbazone on Antioxidan Vitamins in Liver, Kidney And Serum Of Rabbits. NWSA Academic Journals. 2018;13(1):1-6.
17. White R. Applications of Chromatography/Fourier Transform Infrared Spectroscopy. Chromatography/Fourier Transform Infrared Spectroscopy and Its Applications: CRC Press; 2020. p. 235-320.
18. Chemistry of Heterocyclic Compounds: Wiley; 2007.
19. Kwan EE, Huang SG. Structural Elucidation with NMR Spectroscopy: Practical Strategies for Organic Chemists. European Journal of Organic Chemistry. 2008;2008(16):2671-2688.
20. Yu J, Hu DH, Barbara PF. Photophysics of Conjugated Polymers Unmasked by Single Molecule Spectroscopy. Springer Series in Chemical Physics: Springer Berlin Heidelberg; 2001. p. 114-129.
21. Jamel HO, Jasim MH, Mahdi MA, Ganduh SH, Batool M, Jasim LS, et al. Adsorption of Rhodamine B dye from solution using 3-((1-(4-((1H-benzo[d]imidazol-2-yl)amino) phenyl)ethylidene)amino)phenol (BIAPEHB)/ P(AA-co-AM) composite. Desalination and Water Treatment. 2025;321:101019.
22. Majeed HJ, Idrees TJ, Mahdi MA, Abed MJ, Batool M, Yousefi SR, et al. Synthesis and application of novel sodium carboxy methyl cellulose-g-poly acrylic acid carbon dots hydrogel nanocomposite (NaCMC-g-PAAc/ CDs) for adsorptive removal of malachite green dye. Desalination and Water Treatment. 2024;320:100822.
23. Liu H, Li Y, Xiao S, Gan H, Jiu T, Li H, et al. Synthesis of Organic One-Dimensional Nanomaterials by Solid-Phase Reaction. Journal of the American Chemical Society. 2003;125(36):10794-10795.
24. Rodríguez MR, Balsa LM, Piro OE, Etcheverría GA, García-Tojal J, Pis-Diez R, et al. Synthesis, Crystal Structure, Spectroscopic Characterization, DFT Calculations and Cytotoxicity Assays of a New Cu(II) Complex with an Acylhydrazone Ligand Derived from Thiophene. Inorganics. 2021;9(2):9.
25. Kianipour S, Razavi FS, Hajizadeh-Oghaz M, Abdulsahib WK, Mahdi MA, Jasim LS, et al. The synthesis of the P/N-type NdCoO3/g-C3N4 nano-heterojunction as a high-performance photocatalyst for the enhanced photocatalytic degradation of pollutants under visible-light irradiation. Arabian Journal of Chemistry. 2022;15(6):103840.
26. Hosseini M, Ghanbari M, Dawi EA, Mahdi MA, Ganduh SH, Jasim LS, et al. Investigations of nickel silicate for degradation of water-soluble organic pollutants. Int J Hydrogen Energy. 2024;61:307-315.
27. Batool M, Haider MN, Javed T. Applications of Spectroscopic Techniques for Characterization of Polymer Nanocomposite: A Review. Journal of Inorganic and Organometallic Polymers and Materials. 2022;32(12):4478-4503.
28. Shah A, Arjunan A, Manning G, Batool M, Zakharova J, Hawkins AJ, et al. Sequential novel use of Moringa oleifera Lam., biochar, and sand to remove turbidity, E. coli, and heavy metals from drinking water. Cleaner Water. 2024;2:100050.
29. Kim DS, Han SJ, Kwak S-Y. Synthesis and photocatalytic activity of mesoporous TiO2 with the surface area, crystallite size, and pore size. Journal of Colloid and Interface Science. 2007;316(1):85-91.
30. Mahdi MA, Oroumi G, Samimi F, Dawi EA, Abed MJ, Alzaidy AH, et al. Tailoring the innovative Lu2CrMnO6 double perovskite nanostructure as an efficient electrode materials for electrochemical hydrogen storage application. Journal of Energy Storage. 2024;88:111660.
31. Sajeesh S, Sharma CP. Mucoadhesive hydrogel microparticles based on poly (methacrylic acid-vinyl pyrrolidone)-chitosan for oral drug delivery. Drug Deliv. 2010;18(4):227-235.
32. Desai N, Rana D, Salave S, Benival D, Khunt D, Prajapati BG. Achieving Endo/Lysosomal Escape Using Smart Nanosystems for Efficient Cellular Delivery. Molecules. 2024;29(13):3131.
33. Hmood KS, Kubba AARM, Al-bayati RI, Saleh AM. Am Synthesis, Docking Study and In vitro Anticancer Evaluation of Some New Flurbiprofen Derivatives Against MCF-7 and WRL-68 Cell Lines. Indonesian Journal of Pharmacy. 2021.
34. Atyaa AI, Radhy ND, Jasim LS. Synthesis and Characterization of Graphene Oxide/Hydrogel Composites and Their Applications to Adsorptive Removal Congo Red from Aqueous Solution. Journal of Physics: Conference Series. 2019;1234(1):012095.
35. Bayramov A. Environmental Regionalism in the Caspian Sea: A Functionalist Approach. Globalizing Regionalism and International Relations: Policy Press; 2021. p. 103-124. http://dx.doi.org/10.1332/policypress/9781529217148.003.0005
36. Mahde BW, Sultan AM, Mahdi MA, Jasim LS. Kinetic Adsorption and Release Study of Sulfadiazine Hydrochloride Drug from Aqueous Solutions on GO/P(AA-AM-MCC) Composite. International Journal of Drug Delivery Technology. 2022;12(04):1583-1589.
37. Li J, Wei S, Marabada D, Wang Z, Huang Q. Research Progress of Natural Matrine Compounds and Synthetic Matrine Derivatives. Molecules. 2023;28(15):5780.
38. Mahmood Taher A, Ali Kadhim Kyhoiesh H, Shakir Waheeb A, Al-Adilee KJ, Jasim LS. Synthesis, characterization, biological activity, and modelling protein docking of divalent, trivalent, and tetravalent metal ion complexes of new azo dye ligand (N,N,O) derived from benzimidazole. Results in Chemistry. 2024;12:101911.
39. Jayashree BS, Patel HH, Mathew NS, Nayak Y. Synthesis of newer piperidinyl chalcones and their anticancer activity in human cancer cell lines. Res Chem Intermed. 2015;42(4):3673-3688.
40. Kareem Hamzah S. Study some biochemical parameters in pregnant women with hypertension. Journal of Physics: Conference Series. 2019;1234(1):012092.
41. Spectrophotometric Determination of Metoclopramide- HCl in the standard raw and it compared with pharmaceuticals. Journal of Pharmaceutical Negative Results. 2021;21(2).